

Structural basis for the hydrolytic dehalogenation of the fungicide chlorothalonil[†]

Daniel S. Catlin^{3‡}, Xinhang Yang^{1‡}, Brian Bennett², Richard C. Holz^{1,4*}, and Dali Liu^{3*}

¹Department of Chemistry, Marquette University, PO Box 1881, Milwaukee, Wisconsin 53201-1881,

²Department of Physics, Marquette University, 1420 W. Clybourn St., Milwaukee, Wisconsin 53233, the

³Department of Chemistry and Biochemistry, Loyola University Chicago, 1068 W. Sheridan Rd., Chicago, IL 60626, and the ⁴Department of Chemistry, Colorado School of Mines, Golden, Colorado 80401

Running Title: Hydrolytic Dehalogenase from *Pseudomonas* sp. CTN-3 ‡ These authors contributed equally.

To whom correspondence should be addressed: Dali Liu, Department of Chemistry and Biochemistry, Loyola University Chicago, IL 60660, dliu@luc.edu or Richard C. Holz, Department of Chemistry, Colorado School of

Mines, Golden, Colorado 80401, Phone (303) 273-3003, E-mail: rholtz@mines.edu [†]This work was supported by National Science Foundation Grant CHE-1808711 (to B. B. and R. C. H.).

Keyword: Dehalogenase, dechlorination, crystal structure, zinc-dependent, Chd, bioremediation, chlorothalonil, enzyme catalysis, enzyme mechanism, chlorinated aromatic hydrocarbon

Abstract

Cleavage of aromatic carbon–chlorine bonds is critical for the degradation of toxic industrial compounds. Here, we solved the X-ray crystal structure of chlorothalonil dehalogenase (Chd) from *Pseudomonas* sp. CTN-3, with 15 of its N-terminal residues truncated (Chd^T), using single-wavelength anomalous dispersion refined to 1.96 Å resolution. Chd has low sequence identity (< 15%) compared with all other proteins whose structures are currently available, and to the best of our knowledge, we present the first structure of a Zn(II)-dependent aromatic dehalogenase that does not require a coenzyme. Chd^T forms a “head-to-tail” homodimer, formed between two α -helices from each monomer, with three Zn(II)-

binding sites, two of which occupy the active sites, while the third anchors a structural site at the homodimer interface. The catalytic Zn(II) ions are solvent-accessible via a large hydrophobic (8.5 × 17.8 Å) opening to bulk solvent and two hydrophilic branched channels. Each active-site Zn(II) ion resides in a distorted trigonal bipyramidal geometry with His-117, His-257, Asp-116, Asn-216, and a water/hydroxide as ligands. A conserved His residue, His-114, is hydrogen-bonded to the Zn(II)-bound water/hydroxide and likely functions as the general acid–base. We examined substrate binding by docking chlorothalonil (TPN) into the hydrophobic channel and observed that the most energetically favorable pose includes a TPN orientation that coordinates to the active-site Zn(II) ions via a CN and that maximizes a π – π interaction with Trp-227. On the basis of these results, along with previously reported kinetics data, we propose a refined catalytic mechanism for Chd-mediated TPN dehalogenation.

Introduction

Chlorinated aromatic hydrocarbons such as polychlorinated biphenyl, chlorobenzenes and atrazine are important industrial starting materials for the manufacture of dyes, drugs, and pesticides/fungicides

(1,2). Aromatic carbon-chlorine bonds are typically very stable and hence, these compounds persist in soil and contaminate groundwater. Their low water solubility coupled with their toxicity, make them particularly important targets for environmental remediation (3). Enzymatic dehalogenation of chlorinated natural organic matter by organohalide-respiring bacteria provides more soluble compounds that are less likely to bioaccumulate and more likely to be susceptible to further degradation or cellular recycling and thus, less toxic (4-6). Therefore, cleavage of aromatic carbon-chlorine bonds is critical for the degradation of toxic industrial compounds. While enzymatic dehalogenation offers a possible bioremediation solution for chlorinated aromatic compounds, a major impediment to understanding their biological role and bioremediation uses, is the lack of a detailed understanding of their catalytic mechanisms.

The prevailing dogma is that biological dechlorination reactions are catalyzed by either oxidative, reductive, or thiolytic dehalogenation processes (7-13). A relatively unknown biological dehalogenation process involves hydrolysis of a C-Cl bond (14). The chlorothalonil dehalogenase from *Pseudomonas* sp. CTN-3 (Chd) is a Zn(II)-dependent hydrolytic dehalogenase that selectively substitutes an aromatic chlorine-carbon moiety in chlorothalonil (TPN; 2,4,5,6-tetrachloroisophthalonitrile) to an aromatic alcohol (4-hydroxytrichloro-isophthalonitrile; 4-OH-TPN) (Figure 1) (15). TPN is one of the most commonly used fungicides in the US with more than five million kilograms sprayed on crops and fruits each year (16-19). TPN has low solubility in water (100 mg L^{-1}) but is strongly absorbed in soil, particularly soil with high organic matter such as those found in aquatic environments.

TPN is highly toxic to fish and aquatic species as well as birds and invertebrates (1,20,21). TPN is also a human skin and eye irritant that can cause severe gastrointestinal issues. Animal studies involving mice have shown that TPN can cause kidney cancer, so it has been classified by the U.S. Environmental Protection Agency (EPA) as a probable human carcinogen (18). Given the widespread use of TPN and its toxicity, its biodegradation and environmental clean-up has become a topic of significant importance (22).

Several bacterial strains harbor Chd genes that exhibit remarkable sequence identity (>95%) (23-26). Chd was suggested to contain a conserved Zn(II)-binding domain similar to enzymes in the metallo- β -lactamase (MBL) superfamily and was proposed to be dimeric in solution (21). While Zn(II) is required for Chd activity (26), its catalytic role remains unknown. A major limitation in understanding the catalytic mechanism of Chd, and in developing small molecule catalysts that specifically target TPN, is a lack of knowledge regarding its structure and active site architecture. The only aromatic hydrolytic dehalogenase that has been structurally characterized to date is atrazine chlorohydrolase from *Pseudomonas* sp. (AtzA; PDB: 4V1X at 2.2 \AA), which contains an iron ion coordinated by four histidine residues, an aspartate and a water molecule (27). While both AtzA and Chd hydrolytically dehalogenate aromatic compounds, they have relatively low sequence identity (>19%) and different metal ion requirements. Moreover, AtzA is hexameric while Chd is dimeric (15,27).

Herein, we report the 1.96 \AA X-ray crystal structure of a fifteen residue N-terminal truncated Chd enzyme that is fully active, using single wavelength anomalous dispersion (SAD). A truncated form of Chd (Chd^T), which lacked the first fifteen N-terminal residues, was designed and utilized due to poor solubility and stability of the wild-type Chd enzyme at concentrations required for crystallization. The X-ray structure reveals that Chd is a homodimer with a structural Zn(II) residing at the dimer interface and a mononuclear, trigonal bipyramidal (TBP) Zn(II) active site with His117, His257, Asp116, Asn216, and water/hydroxide as ligands. Based on this structure, substrate modeling, and previous kinetic studies (26), a refined catalytic mechanism is proposed.

Results

Overall structure of Chd^T. Chd^T crystals with dimensions 0.1 mm x 0.2 mm x 0.3 mm belonged to the primitive orthorhombic space group P2₁2₁2₁ with unit cell parameters a = 90 Å, b = 80 Å, and c = 90 Å. The structure was solved via SAD using a wavelength of 1.28 Å, close to the absorption edge of Zn. The final model was re- refined to a resolution of 1.96 Å with R_{free} and R_{work} values of 19.80% and 16.22%, respectively. Final data processing and refinement statistics are listed in Table 1. A single homodimer was built in an asymmetric unit. The final refined model has been deposited to the Protein Data Bank (PDB) as PDB code: 6UXU.

The two monomers of the homodimer display a two-fold non-crystallographic rotational axis that passes through a non-catalytic structural Zn(II) site (Figure 2A). From a side view (Figure 2B), the structural Zn(II) ion is close to one side of the dimer surface. For convenience purposes, we refer to this side of the dimer protein as the “top” side i.e. where the structural Zn(II) ion resides and the opposite side to as the “bottom”. The crystallographic packing was analyzed using PISA (28,29) in the CCP4 suite and the observed homodimer in the asymmetric unit was predicted by PISA to be the only stable quaternary structure in solution. The total predicted accessible surface area (ASA) is 23,000 Å², while the predicted buried surface area (BSA) is 1,800 Å².

Each monomer contains a catalytic Zn(II) ion that is solvent-accessible from both the “top” and the “bottom” sides of the protein (Figure 3). From the “bottom”, a “Y” shaped channel exists with two branched channels that lead to the catalytic Zn(II) ions and share a single large (8.5 x 17.8 Å) opening to bulk solvent. On the other hand, the structural Zn(II) ion is not accessible to the bulk solvent despite being located close to the “top” side surface. From the “top” side, the structural features surrounding the structural Zn(II) ion help to form two bent channels that provide access the catalytic Zn(II) ions.

The monomer protein fold is an αββα-sandwich. The overall protein fold of the Chd^T monomer (Figure 4A) was searched using the D.A.L.I. server (30) for comparison against all known structures. Interestingly, known structures with any similarity to Chd were reported as either β-lactamases or alkylsulfatases (31-34). The most similar structures from each of these protein families, CphA, and Pisa1, were selected for detailed comparison and structurally aligned with Chd^T (Figures 4B and 4C). The overall fold of the Chd^T monomer aligned well with the overall structure of the β-lactamase, CphA (PDB Code: 3IOG), except for an extra C-terminal motif in Chd^T. The N-terminal portion (residues 1-277) of Chd forms an αββα-sandwich fold that is commonly observed in the β-lactamase superfamily; however, Chd^T also possessed an additional C-terminal motif (residues 278-327) that originates in the middle of a long helix that is not found in the CphA structure. On the other hand, when Chd^T was structurally aligned with one subunit of the alkylsulfatase, Pisa1 (PDB Code: 2YHE), the additional C-terminal motif observed in Chd^T was present in Pisa1, which is much larger in size than either Chd or CphA.

The active site of Chd. The coordination geometry of the active site Zn(II) ion is identical in both monomers and the simulated annealing composite omit map around each metal ion and their coordinating residues are consistent with the active site Zn(II) ion residing in a distorted trigonal bipyramid or TBP geometry (Figure 5A). The catalytic Zn(II) ion ligands include the N^ε nitrogens of His117 (2.0 Å) and His257 (2.0 Å) along with a water/hydroxide oxygen atom (2.6 Å) making up the equatorial positions, while a carboxylate oxygen atom of Asp116 (2.1 Å) and a carbonyl oxygen atom of Asn216 (2.2 Å) (Table 2; Figure 5A) constitute the axial ligands. The coordinating water/hydroxide forms hydrogen bonds with the axial ligands Asp116 (2.6 Å) and Asn216 (2.9 Å) (Figure 5A). Another active site residue, His114, is observed in two alternate conformations supported by simulated annealing composite omit maps (Figures 5B). In one conformation (a), the N^ε nitrogen atom of the imidazole ring is hydrogen bound to the coordinated water/hydroxide oxygen atom (2.9 Å) and the nitrogen atom (2.7 Å) of the axial ligand, Asn216. The second conformation (b) places the imidazole ring perpendicular to the imidazole ring in the (a) conformation resulting in the loss of hydrogen bonding interactions with both

the coordinated water/hydroxide oxygen atom (5.4 Å) and possibly the nitrogen atom (3.1 Å) of the axial ligand Asn216. The structural Zn(II) ion is coordinated by the N^ε nitrogen atoms of His143 (2.0 Å) and the carboxylate oxygen atom of Asp146 (1.9 Å) from each subunit (Figure 5C and 5D), providing a tetrahedral coordination geometry.

Role of the structural Zn(II) site. The structural Zn(II) site ligands were eliminated by mutating both His143 and Asp146 to Ala. Removal of the structural Zn(II) site ligands had no apparent effect on Chd^T activity as the double mutant exhibited a k_{cat} of 25 ± 1 , which is identical to that of wild-type Chd (15,26). Surprisingly, homodimer formation was also not affected based on gel filtration results (Supporting Information Figure SI1). However, elimination of the structural Zn(II) site did increase the K_m value 2-fold ($K_m = 0.24 \pm 0.07 \mu\text{M}$) and severely affected protein stability as the purified mutant protein precipitated within ~2 hours when incubated at 23 to 25 °C.

Chd biological assembly in solution. The intact molecular masses of both the truncated and structural Zn(II) Chd mutants were obtained by MALDI-TOF Mass Spectrometry (Figure 6). Masses consistent with homodimer formation were observed between 66 and 70 kDa. These MS data are consistent with the hydrodynamic volume for both samples determined by size exclusion chromatography (Supporting Information Figure SI1), which indicate a molecular weight consistent with a homodimer in solution. It should also be noted that a small portion of Chd^T fragmented (<8%) during MALDI-TOF MS analysis.

Substrate docking. Attempts to co-crystallize or soak crystals of Chd^T with the substrate TPN or recently identified inhibitors, were unsuccessful; therefore, substrate docking was utilized to examine possible substrate binding poses. Substrate docking generated four different poses ranked by the docking scoring function, where a lower value indicates lower total energy after docking (Figure 7) (35-37). The top ranked model (#1) suggested a binding interaction between the nitrogen atom of a cyano group of TPN and the active site Zn ion (2.3 Å), along with an energetically favorable π - π interaction between the TPN aromatic ring and that of the active site residue Trp227. Interestingly, this pose pre-organizes a possible transition state of TPN hydrolysis by placing the ortho carbon of TPN within ~3.0 Å of the O atom of the bound water/hydroxide. In each of the other poses, all possible TPN ligating groups are too far from the catalytic Zn(II) ion to be considered a bonding interaction (>3.5 Å). However, model (#3) revealed a hydrogen bond between the nitrogen atom of a TPN cyano group and the amide nitrogen of the Zn(II) ligands Asn216 (2.3 Å). The resulting substrate position placed the ortho carbon of TPN within 3.1 Å of the O atom of the bound water/hydroxide. In contrast to model (#1), TPN is rotated in this pose, which abolished the energetically favorable π - π interaction between the TPN aromatic ring and that of Trp227.

Discussion

Chd is a protein with an unusual sequence: the highest sequence similarity to a structurally characterized protein, glyoxylase II from *Araobidopsis thaliana* (PDB IXM8), is 14.7%. Here, a 1.96 Å-resolution structure of Chd^T, a truncated construct of Chd, is reported that reveals an $\alpha\beta\beta\alpha$ -sandwich fold that is also observed in the metallo- β -lactamase (MBL) superfamily (38). Chd is a “head-to-tail” homodimer, formed between two α -helices from each monomer (Figure 4). Each monomer contains a mono-Zn(II) active site, and a third Zn(II) ion anchors an intersubunit structural site. Otherwise, and uniquely for enzymes with the same functionality, no coenzyme is associated with active Chd.

The mononuclear Zn(II) active site in each monomer of Chd is a characteristic shared with the B2 metallo- β -lactamases. The third Zn(II) ion in the Chd homodimer, which is coordinated by the N^ε nitrogen atom of a His143 and a carboxylate oxygen atom of Asp146 from each subunit, resides in a tetrahedral coordination geometry that is buried at the dimer interface and likely functions as a structural site. A

Chd^{T(H143A, D146A)} construct predictably lacked the ability to bind this third zinc ion but, surprisingly, exhibited full catalytic activity, albeit with a two-fold elevated K_m . Additionally, the Chd^{T(H143A, D146A)} variant re-tained the homodimeric architecture of the native protein in solution. The most striking effect of the double mutation was markedly impaired stability in solution at ambient temperatures.

The X-ray structure of Chd revealed two previously unknown solvent accessible channels in each monomer that likely provide different routes for substrate and products to access/leave the catalytic Zn(II) site (Figure 3). As TPN is hydrophobic in nature, hydrolysis of an ortho-chlorine produces more hydrophilic products: 4-OH-TPN, a chloride ion and a proton. As the products of TPN hydrolysis vary greatly in solubility and size, it would be reasonable to have two sets of solvent channels capable of shuttling different reactants and products to and from the active site. The “Y” shaped channel that originates on the “bottom” of the Chd homodimer contains a large opening (8.5 x 17.8 Å) with a channel that is largely hydrophobic. This “Y” shaped channel likely serves to recognize substrate and guide TPN to the active site. On the other hand, water and H⁺ and/or chloride ions can migrate through the second active site channel, which is more hydrophilic, and resides on the “top” side of the dimer. It has been reported that dimerization of SidA, which is an alkylsulfatase similar to Pisa1, ensures resistance to biocidal SDS at toxic concentrations (39). Given that TPN is toxic, Chd may have evolved as a dimer with two active site channels to elicit a similar response.

As predicted by Wang et al. (15), the first His in the B2 β -lactamase MBL (His-X-His-Asp-His) is replaced by a Ser (Ser112 in Chd). This minor change in the B2 β -lactamase MBL active site may explain why a dinuclear Zn(II) site does not occur in both B2 enzymes and Chd. The single active site Zn(II) ion in Chd resides in a distorted trigonal bipyramid (TBP) geometry with His117, His257, Asp116, Asn216, and water/hydroxide as ligands (Figure 5). Several potentially important hydrogen-bonding interactions also exist in the active site of Chd. Perhaps most notably, there is at least one interaction between the metal bound water/hydroxide oxygen atom and the N^ε nitrogen atom of His114. His114 forms a strong hydrogen bond (~2.9 Å) with the equatorial metal bound water/hydroxide in Chd and also with the nitrogen atom of the axial Asn216 ligand (~2.7 Å). Interestingly, His114 clearly occupies two orientations in the structure, the second of which is perpendicular to the hydrogen bond conformation, which places the N^ε nitrogen atom out of hydrogen bonding range of the metal-bound water/hydroxide (~5.4 Å), but close enough to the axial ligand Asn216 (~3.1 Å) to possibly form a hydrogen bond. The functional role of His114

and its flexibility is currently unknown but may play a catalytic role as a general acid/base. This is consistent with both ChpA and Pisa1, as His114 is strictly conserved in both enzymes and in ChpA, it was also proposed to be the general acid to protonate the leaving group (40).

Other potentially important hydrogen bonding interactions occur between the Asn216 carboxamide nitrogen proton and the metal bound water/hydroxide (2.9 Å) and the second axial Asp116 ligand carboxylate oxygen, also with the metal bound water/hydroxide (2.6 Å). These hydrogen bonding interactions likely assist in the deprotonation of the bound water to a nucleophilic hydroxide. Finally, a potentially important hydrogen bonding interaction occurs between the N^δ proton of the His117 ligand with a side chain oxygen atom of Glu81 (~2.7 Å) forming a Glu-His-Zn triad that has been postulated to decrease the Lewis acidity of zinc ions,(41) and may further assist in facilitating the coordination of substrate or water to the active site Zn(II) ion. Similar arrangements and fully conserved Asp-His-Zn triads are observed for other hydrolases (42).

The discovery of a large hydrophobic channel on the “bottom” of the Chd homodimer that provides access to the catalytic Zn(II) ion, suggests that it may serve as the initial substrate recognition site. To properly position an aromatic substrate, such as TPN, for catalysis the substrate would need to either

bind to or near the active site Zn(II) ion. Interestingly, Trp227 resides in the hydrophobic channel ~ 9.1 Å from the active site metal ion. Previous mutagenesis studies indicated that Trp227 is catalytically essential (15), suggesting that it may be involved in recognizing and positioning TPN near the active site Zn(II) ion via a π - π interaction. To test this hypothesis, TPN was docked into the hydrophobic channel with the most energetically favorable pose occurring for a TPN orientation that maximizes the π - π interaction with Trp227, places a CN nitrogen atom within a bonding distance to the active site Zn(II) (~ 2.3 Å), and expands its coordination geometry to octahedral (Figure 7; Pose #1). As the C4 and C6 chlorines in TPN are chemically equivalent (homotopic) given the symmetry arising from the positions of the two CN substitutes, it does not matter which CN group binds to the active site Zn(II) ion. Chd catalyzes the dehalogenation of only one chlorine and the resulting product cannot serve as a substrate for Chd. In pose #1, the C4/C6 chlorine would be positioned so that once the hydrolysis reaction occurs, the newly formed chloride ion would be oriented towards the small backend channel for expulsion to the bulk solvent. While a second pose was reasonably energetically favorable (Figure 7; Pose #2), TPN was rotated thus abolishing the energetically favorable π - π interaction between the TPN aromatic ring and that of Trp227. However, this pose does reveal a potential hydrogen bond between the nitrogen atom of a TPN cyano group and the amide nitrogen Asn216, which places the ortho carbon of TPN within 3.1 Å of the O atom of the bound water/hydroxide.

In conclusion, the X-ray crystal structure of Chd^T, in combination with previously reported kinetic data allows us to refine our proposed catalytic mechanism for Chd (Figure 8) (26). The first step in catalysis is likely recognition of TPN by the large hydrophobic channel that leads to the Zn(II) active site. In this scenario, TPN is positioned by a π - π interaction with Trp227 that was shown to be important for catalytic turnover (15). Next, a CN nitrile nitrogen atom of TPN coordinates to the active site Zn(II), although no direct evidence exists to support this assumption at this time, expanding its coordination number from five to six. Binding of the substrate nitrile nitrogen has a two-fold impact. First, it removes electron density from the aromatic ring activating the ortho carbon for nucleophilic attack (27,43), and second, it activates the coordinated water/hydroxide to function as a nucleophile. Deprotonation of the metal-bound water molecule by His114, with assistance from the Zn(II) ligands Asp116 and Asn227, forms a nucleophilic hydroxide moiety that is consistent with the postulated pK_a of the zinc-bound water molecule (44). Once the zinc-bound hydroxide is formed, it can attack the activated ortho carbon of TPN, forming an η -1- μ -transition-state complex (45). Solvent kinetic isotope effect studies indicate that one proton is transferred in the transition-state, likely due to the breaking of a water O-H bond and the formation of a protonated His114 (26). The observed conformational flexibility of His114 may facilitate the formation of products and enable their release. Once the products are released, the Zn(II)-bound water molecule is replaced. While a mechanism could also be proposed where a nitrile nitrogen atom of TPN does not bind to the active site Zn(II) ion, there is no residue other than the Zn(II) ligand Asn216 that could reasonably form a hydrogen bond to the nitrile nitrogen of TPN, which would be important for activating the substrate for hydrolysis.

Experimental Procedures

Materials. NEB restriction enzymes, T4 DNA Ligase, Agilent QuikChange II site-directed mutagenesis kit, Ni-NTA columns, Wizard® SV gel and PCR clean-up systems, size exclusion columns 4-(2-hydroxyethyl)-1-piperazineethanesulfonic acid, potassium bromide, potassium sodium tartrate, and TPN were purchased commercially (Fisher Scientific, WI) at the highest purity available. TEV protease (EC 3.4.22.44) was obtained via previously published methods (46).

N-terminal sequence modification of Chd. The first fifteen residues of the N-terminus of WT Chd were removed by PCR (sense primer: ACTCCATGGATGCCGTGAAATTTAG, anti-sense primer: CATAAGCTTTTAATGGTGATGGTGATGGTGATG). The modified Chd gene containing NcoI and

HindIII restriction sites was amplified under standard PCR conditions for gene cloning (47). The PCR products were purified by agarose gel electrophoresis and Wizard SV gel and subcloned into pET28a+, creating the new expression vector pET28a+-Chd . The modified sequence was verified by Functional Biosciences (Madison, WI.).

Expression and Purification of Chd^T . The plasmid containing Chd^T was freshly transformed into BL21(DE3) competent cells (Stratagene), and a single colony was used to inoculate 50 mL of LB-Miller culture containing 50 µg/mL kana- mycin with shaking overnight at 37 °C as previously described (26). Briefly, this culture was used to inoculate a 1 L culture and the cells were grown at 37 °C until an OD_{600nm} of 0.8-1.0 was reached. The culture was cooled on ice, induced with 0.1 mM isopropyl β-D-1-thiogalactopyranoside (IPTG) supplemented with 0.05 mM ZnCl₂, and expressed at 25 °C for 16 hours. Cells were harvested by centrifugation at 6,370 x g and 4 °C for 10 min in a Beckman Coulter Avanti JA- 10 rotor and resuspended in 20 mM Tris-HCl buffer, pH 7.0 containing 50 mM NaCl, 10 mM TCEP, and 25 mM imidazole at a ratio of 5 ml per gram of cells. Cells were lysed by ultrasonication (Misonix Sonicator 3000) for 4 min (30 s on 45 s off) at 21 W. The crude extract was obtained after centrifugation in a JA-20 rotor at 31,000 x g and 4 °C for 20 min.

Crude extracts of Chd^T (100 mg) were loaded onto a 5 ml Ni-NTA (nitrilotriacetic acid) Super-flow Cartridge (Qiagen) using an ÄKTA FPLC P- 960. The column was washed with 50 mL of 20 mM Tris-HCl buffer, pH 7.0 containing 50 mM NaCl and 25 mM imidazole, followed by 50 mL of 20 mM Tris-HCl buffer, pH 7.0 containing 50 mM NaCl and 75 mM imidazole. The protein was eluted using a linear imidazole gradient (75 to 500 mM) at a flow rate of 2 mL/min. Active protein fractions were pooled and concentrated using 50 mM Tris buffer, pH 7.0 containing 1 mM EDTA with an Amicon Ultra-15 10,000 MWCO centrifugal filter unit (Millipore) resulting in ~12 mg/L of soluble Chd^T-His₆. The His₆-tag was removed by treating His₆- tagged Chd^T with His₆-tagged TEV protease (EC3.4.22.44) for 16 h at 4 °C in 50 mM Tris, pH 8.0. Cleaved protein was concentrated with a Centri-

con (15,000-MW cutoff; Amicon) to 3 mL and loaded on IMAC to remove the remaining cleaved His₆-tag, uncut protein and the His₆-tagged TEV protease, while the flow through containing Chd^T was collected and washed with 50 mM HEPES buffer, pH 7.0 containing 10% glycerol. Purified protein was analyzed by SDS-PAGE with a 12.5% polyacrylamide SPRINT NEXT GEL™ (Amresco). Gels were stained with Gel Code Blue (Thermo-Fisher Scientific). Protein concentration of crude extracts was determined using a Coomassie (Bradford) Protein Assay Kit (Pierce) and pure protein by measuring the absorbance at 280 nm with a Shimadzu UV-2450 spectrophotometer equipped with a TCC-240A temperature-controlled cell holder. Theoretical molecular weights and protein extinction coefficients were calculated with the ExPASy compute pI/Mw tool.

Activity assay of Chd^T . The enzymatic activity of Chd^T towards TPN was measured using a Shimadzu UV-2450 spectrophotometer equipped with a TCC-240A temperature-controlled cell holder in 1 mL quartz cuvettes. A 1 mL reaction consisted of 50 mM HEPES buffer, pH 7.0 at 25 °C and various concentrations of TPN. The rate of TPN dehalogenation was determined by continuously monitoring the formation of 4-OH-TPN at 345 nm ($\Delta\epsilon_{345} = 3.5 \text{ mM}^{-1}\text{cm}^{-1}$). Data analysis was performed using OriginPro 9.0 (OriginLab, Northampton, MA). The kinetic constants V_{max} and K_m were calculated by fitting to the Michaelis-Menten equation. One unit of enzyme activity was defined as the amount of enzyme that catalyzed the production of 1 µmol of the TPN minute at 25 °C.

Crystallization. Purified Chd^T was exchanged into 50 mM HEPES buffer, pH 7.5 containing 10% glycerol for crystallization and concentrated to a final protein concentration of 10 mg/mL. Initial crystallization screens using a Gryphon Crystallization Robot (Art Robins Inc.) and Emerald Biosystems

Wizard III/IV screen sets, produced crystals of Chd^T in 10% PEG 6000 and 100 mM HEPES buffer, pH 7.0. Crystallization optimization leads revealed the best quality Chd^T crystals via sitting drop vapor diffusion occurred by mixing 6 μ L of (10 mg/mL) Chd^T with 6 μ L of well solution (10% PEG 6000, 100 mM HEPES, pH 7.0). Crystals were allowed to grow at room temperature and reached optimal size and morphology for data collection after 7-10 days. Crystals were manually transferred to well solution supplemented with 30% Glycerol (cryoprotectant) and flash frozen in liquid N₂.

X-ray diffraction data collection. Single wavelength anomalous dispersion (SAD) and monochromatic data were collected at the LS-CAT 21-ID Advanced Photon Source (APS) at Argonne National Laboratory (ANL). SAD data sets were collected at a wavelength of 1.28 Å while another monochromatic data set was collected at 0.98 Å at 100 K using a Dectris Eiger 9M detector. Data sets were indexed and integrated using the HKL2000 suite.

Model Building and Refinement. The structure of Chd^T was solved by single wavelength anomalous dispersion (SAD) using autosol in the Phenix software suite (48). The model building was first conducted in autobuild followed by COOT (49), refined using Phenix, and analyzed in COOT and USCF Chimera (50). Final refinement statistics are reported in Table 1 and structural figures were made using USCF Chimera.

Double mutation at the structural zinc binding site. His143 and Asp146, structural Zn(II) site ligands, were mutated to alanine (Ala143 and Ala146) by a single mutagenic primer as follows: Sense primer: TTGATGGTGCCCTGGCGGC- CGATAAGGCGTTCATGGT, antisense primer: ACCATGAACGCCTTATCGGCCGCCAGGGC ACCATCAA. Mutated residues are shown in bold. The sense primer had a completely complementary sequence to the corresponding antisense primer. The first PCR reaction was performed using sense primer and antisense primer in separate tubes (25 μ L). Following denaturation at 98 °C for 1 min, 5 PCR cycles were carried out with each cycle comprised of incubation at 98 °C for 15 s, followed by a 30 s annealing step at 65 °C, and a 1 min. extension at 71 °C. A 50 μ L solution was prepared by combining two tubes for a second PCR reaction, which was carried out under the same conditions as the first PCR reaction but for 55 cycles. The final products were transformed directly into XL10-gold ultracompetent cells. The mutated Chd^T sequence was verified by DNA sequencing by Functional Biosciences (Madison, WI.)

MALDI-TOF mass spectrometry. Saturated α -CHCA thin layer solution was prepared on a MALDI target (51). A 2 μ L protein sample (10 μ M) was mixed with a DHB-CHCA matrix on a MALDI target by the “sandwich method” (52). Mass spectra of each sample were obtained on a Bruker microflex LRFTM MALDI-TOF Mass spectrometer.

Substrate docking. TPN poses were created and optimized by Molecular Operating Environment (Chemical Computing Group, Montreal, Canada). The TPN substrate was docked into the Chd^T active site pocket using Autodock Vina, which is a structural analysis panel of Chimera 1.13.1rc (UCSF Chimera, San Francisco, CA). The optimized TPN molecule was deemed a ligand while the active site of Chd was assigned as a receptor. The oxygen position of the active site Zn(II)-bound water/hydroxide was fixed as were the protein residue ligands. The best pose, based on the docking scoring function vs binding energy (37), was considered the final model.

Data Availability Statement: All data described in the manuscript are contained within the manuscript or the supplementary information. The final refined model was deposited at the Protein Data Bank (PDB; 6UXU).

Acknowledgments: We thank the National Science Foundation (CHE-1808711 BB & RCH) for funding this research. This research used re- sources of the Advanced Proton Source, a U.S. Department of Energy (DOE) Office of Science User Facility operated for the DOE Office of Science by Argonne National Laboratory under contract No. DE-AC02-06CH11357. Use of LS-CAT Sector 21 was supported by the Michigan Economic Development Corporation and the Michigan Technology Tri-Corridor (Grant 085P1000817).

Abbreviations: Chd, chlorothalonil dehalogen- ase; 2,4,5,6-tetrachloroiso-phtalonitrile , TPN; ORF, open reading frame; IMAC, immobilized metal affinity chromatography; Single Wave- length Anomalous Dispersion, SAD, MALDI- TOF, matrix-assisted laser desorption ionization time-of-flight mass spectrometry.

Conflict of interest: The authors declare that they have no conflicts of interest with the con- tents of this article.

Author contributions: XY prepared the gene for Chd^T and the Chd His143 and Asp146 double mutant, carried out protein expression, purifica- tion, enzymatic assays, MOLDI-TOF MS experi- ments, and the substrate docking studies. DSC screened Chd for crystallization and optimized these conditions. DSC collected and processed the crystallographic data, obtained initial phases using SAD, built and refined the final structural model of Chd^T. RCH and BB conceived of the idea while DI oversaw X-ray refinement and RCH, BB, and DI wrote the paper with XY and DSC.

References

1. Sims, J. L., Suflita, J. M., and Russell, H. H. (1991) Reductive Dehalogenation of Organic Contaminants in Soils and Ground Water. (Agency, U. S. E. P. ed., Superfund Technology Support Center for Ground Water
2. Arora, P. K., and Bae, H. (2014) Role of Dehalogenases in Aerobic Bacterial Degradation of Chlorinated Aromatic Compounds. *J. Chem. Dalton Trans.*, 1-11
3. Baxter, J., and Cummings, S. P. (2006) The current and future applications of microorganism in the bioremediation of cyanide contamination. *Antonie Van Leeuwenhoek* 90, 1-17
4. Copley, S. D. (1998) Microbial dehalogenases: enzymes recruited to convert xenobiotic substrates. *Curr Opin Chem Biol* 2, 613-617
5. de Jong, R. M., and Dijkstra, B. W. (2003) Structure and mechanism of bacterial dehalogenases: different ways to cleave a carbon- halogen bond. *Curr Opin Struct Biol* 13, 722-730
6. Janssen, D. B., Oppentocht, J. E., and Poelarends, G. J. (2001) Microbial dehalogenation. *Curr Opin Biotechnol* 12, 254-258
7. Reddy, G. V., and Gold, M. H. (2000) Degradation of pentachlorophenol by *Phanerochaete chrysosporium*: intermediates and reactions involved. *Microbiology* 146 (Pt 2), 405-413
8. Beil, S., Mason, J. R., Timmis, K. N., and Pieper, D. H. (1998) Identification of chlorobenzene dioxygenase sequence elements involved in dechlorination of 1,2,4,5-tetrachlorobenzene. *Journal of bacteriology* 180, 5520-5528
9. Xun, L., Topp, E., and Orser, C. S. (1992) Purification and characterization of a tetrachloro-p-hydroquinone reductive dehalogenase from a *Flavobacterium* sp. *Journal of bacteriology* 174, 8003-8007
10. Orser, C. S., Dutton, J., Lange, C., Jablonski, P., Xun, L., and Hargis, M. (1993) Characterization of a *Flavobacterium* glutathione S- transferase gene involved reductive dechlorination. *Journal of bacteriology* 175, 2640-2644
11. Yokota, T., Fuse, H., Omori, T., and Minora, Y. (1986) Microbial dehalogenation of haloalkanes mediated byoxy genases or halidohydrolase. *Agric. Biol. Chem.* 50, 453-460
12. Bunge, M., , Adrian, L., Kraus, A., Opel, M., Lorenz, W. G., Andreesen, J. R., Görisch, H., and Lechner, U. (2003) Reductive dehalogenation of chlorinated dioxins by an anaerobic bacterium. *Nature* 421, 357-360
13. Leisinger, T., Bader, R., Hermann, R., Schmid-Appert, M., and Vuilleumier, S. (1994) Microbes, enzymes and genes involved in dichloromethane utilization. *Biodegradation* 5, 237-248
14. Ang, T. F., Maingwa, J., Salleh, A. B., Normi, Y. M., and Leow, T. C. (2018) Dehalogenases: From Improved Performance to Potential Microbial Dehalogenation Applications. *Molecules* 23
15. Wang, G., Li, R., Li, S., and Jiang, J. (2010) A novel hydrolytic dehalogenase for the chlorinated aromatic compound chlorothalonil. *J Bacteriol* 192, 2737-2745
16. Caux, P. Y., Kent, R. A., Fan, G. T., and Stephenson G. L. (1996) Environmental fate and effects of chlorothalonil: A Canadian perspective *Crit. Rev. Environ. Sci. Technol.* 26, 45-93

17. Sakkas, V. A., Lambropoulou, D. A., and Albanis, T. A. (2002) Study of chlorothalonil photodegradation in natural waters and in the presence of humic substances. *Chemosphere* 48, 939-945
18. Mozzachio, A. M., Rusiecki, J. A., Hoppin, J. A., Mahajan, R., Patel, R., Beane-Freeman, L., and Alavanja, M. C. (2008) Chlorothalonil exposure and cancer incidence among pesticide applicator participants in the agricultural health study. *Environmental research* 108, 400-403
19. Carlo-Rojas, Z., Bello-Mendoza, R., Figueroa, M. S., and Sokolov, M. (2004) Chlorothalonil Degradation under Anaerobic Conditions in an Agricultural Tropical Soil. *Water, Air, & Soil Pollution* 151, 397-409
20. Vickers, A., Sloop, T., and Lucier, G. (1985) Mechanism of Action of Toxic Halogenated Aromatics. *Environ Health Perspect.* 59, 121-126
21. Wang, G., Li, R., Li, S., and Jiang, J. (2010) A Novel Hydrolytic Dehalogenase for the Chlorinated Aromatic Compound Chlorothalonil. *J. Bacteriol.* 192, 2737-2745
22. Viciu, M. S., Grasa, G. A., and Nolan, S. P. (2001) Catalytic Dehalogenation of Aryl Halides Mediated by a Palladium/Imidazolium Salt System. *Organometallics* 20, 3607-3612
23. Liang, B., Wang, G., Zhao, Y., Chen, K., Li, S., and Jiang, J. (2011) Facilitation of bacterial adaptation to chlorothalonil- contaminated sites by horizontal transfer of the chlorothalonil hydrolytic dehalogenase gene. *Applied and environmental microbiology* 77, 4268-4272
24. Ren, X., Li, H., and Chen, S. (2011) Cloning of the chlorothalonil-degrading gene cluster and evidence of its horizontal transfer. *Current microbiology* 62, 1068-1073
25. Yue, W., Xiong, M., Li, F., and Wang, G. (2015) The isolation and characterization of the novel chlorothalonil-degrading strain *Paracoccus* sp. XF-3 and the cloning of the *chd* gene. *Journal of bioscience and bioengineering* 120, 544-548
26. Yang, X., Bennett, B., Liu, D., and Holz, R. C. (2019) Insights into the Catalytic Mechanism of a Bacterial Hydrolytic Dehalogenase that Degrades the Fungicide Chlorothalonil. *J. Biol. Chem.* 264, 13411-13420
27. Peat, T. S., Newman, J., Balotra, S., Lucent, D., Warden, A. C., and Scott, C. (2015) The structure of the hexameric atrazine chlorohydrolase AtzA. *Acta Crystallogr D Biol Crystallogr* 71, 710-720
28. Krissinel, E. (2010) Crystal contacts as nature's docking solutions. *J Comput Chem* 31, 133-143
29. Krissinel, E., and Henrick, K. (2007) Inference of macromolecular assemblies from crystalline state. *J Mol Biol* 372, 774-797
30. Holm, L., and Laakso, L. M. (2016) Dali server update. *Nucleic Acids Res* 44, W351-355
31. Crowder, M. W., Spencer, J., and Vila, A. J. (2006) Metallo-beta-lactamases: novel weaponry for antibiotic resistance in bacteria. *Acc Chem Res* 39, 721-728
32. Fryszczyń, B. G., Adamski, C. J., Brown, N. G., Rice, K., Huang, W., and Palzkill, T. (2014) Role of beta-lactamase residues in a common interface for binding the structurally unrelated inhibitory proteins BLIP and BLIP-II. *Protein Sci* 23, 1235-1246
33. Knaus, T., Schober, M., Kepplinger, B., Faccinelli, M., Pitzer, J., Faber, K., Macheroux, P., and Wagner, U. (2012) Structure and mechanism of an inverting alkylsulfatase from *Pseudomonas* sp. DSM6611 specific for secondary alkyl sulfates. *Febs J* 279, 4374- 4384
34. Walsh, T. R., Toleman, M. A., Poirel, L., and Nordmann, P. (2005) Metallo-beta-lactamases: the quiet before the storm? *Clin Microbiol Rev* 18, 306-325
35. Quiroga, R., and Villarreal, M. A. (2016) Vina: A Scoring Function Based on Autodock Vina Improves Scoring, Docking, and Virtual Screening. *PLoS One* 11, e0155183
36. Seeliger, D., and de Groot, B. L. (2010) Ligand docking and binding site analysis with PyMOL and Autodock/Vina. *J Comput Aided Mol Des* 24, 417-422
37. Trott, O., and Olson, A. J. (2010) AutoDock Vina: improving the speed and accuracy of docking with a new scoring function, efficient optimization, and multithreading. *J Comput Chem* 31, 455-461
38. Baier, F., and Tokuriki, N. (2014) Connectivity between catalytic landscapes of the metallo-beta-lactamase superfamily. *J Mol Biol* 426, 2442-2456
39. Hagelueken, G., Adams, T. M., Wiehlmann, L., Widow, U., Kolmar, H., Tummler, B., Heinz, D. W., and Schubert, W. D. (2006) The crystal structure of SdsA1, an alkylsulfatase from *Pseudomonas aeruginosa*, defines a third class of sulfatases. *Proc Natl Acad Sci U S A* 103, 7631-7636
40. Garau, G., Bebrone, C., Anne, C., Galleni, M., Frere, J. M., and Dideberg, O. (2005) A metallo-beta-lactamase enzyme in action: crystal structures of the monozinc carbapenemase CphA and its complex with biapenem. *J Mol Biol* 345, 785-795
41. Christianson, D., and Cox, D. (1999) Catalysis by Metal-Activated Hydroxide in Zinc and Manganese Metalloenzymes. *Annu. Rev. Biochem.* 68, 33-57
42. Desmarais, W., Bienvenue, D. L., Bzymek, K. P., Petsko, G. A., Ringe, D., and Holz, R. C. (2006) The High-Resolution Structures of the Neutral and the Low pH Crystals of the Aminopeptidase from *Aeromonas proteolytica*. *J. Biol. Inorg. Chem.* 11, 398-408
43. Hu, J., Su, Q., Schlessman, J. L., and Rokita, S. E. (2019) Redox control of iodotyrosine deiodinase. *Protein Sci* 28, 68-78

44. Sakurai, M., Furuki, T., and Inoue, Y. (1995) The pKa of the zinc-bound water in carbonic anhydrase and its model compounds as studied by the AM1 calculation coupled with a reaction field theory. *The Journal of Physical Chemistry* 99, 17789-17794
45. Cosper, N. J., Bienvenue, D. L., Shokes, J., Gilner, D. M., Tsukamoto, T., Scott*, R., and Holz*, R. C. (2004) The dapE-encoded N- succinyl-L,L-Diaminopimelic Acid Desuccinylase from *Haemophilus influenzae* is a Dinuclear Metallohydrolase. *J. Am. Chem. Soc.* 125, 14654-14655
46. Tropea, J. E., Cherry, S., and Waugh, D. S. (2009) Expression and purification of soluble His(6)-tagged TEV protease. *Methods Mol Biol* 498, 297-307
47. Yang, X., Bennett, B., and Holz, R. C. (2018) Analyzing the function of the insert region found between the alpha and beta-subunits in the eukaryotic nitrile hydratase from *Monosiga brevicollis*. *Arch Biochem Biophys* 657, 1-7
48. Adams, P. D., Afonine, P. V., Bunkoczi, G., Chen, V. B., Davis, I. W., Echols, N., Headd, J. J., Hung, L.-W., Kapral, G. J., Grosse-Kunstleve, R. W., McCoy, A. J., Moriarty, N. W., Oeffner, R., Read, R. J., Richardson, D. C., Richardson, J. S., Terwilliger, T. C., and Zwart, P. H. (2010) PHENIX: a comprehensive Python-based system for macromolecular structure solution. *Acta Crystallographica Section D* 66, 213-221
49. Emsley, P., Lohkamp, B., Scott, W. G., and Cowtan, K. (2010) Features and development of Coot. *Acta crystallographica. Section D, Biological crystallography* 66, 486-501
50. Pettersen, E. F., Goddard, T. D., Huang, C. C., Couch, G. S., Greenblatt, D. M., Meng, E. C., and Ferrin, T. E. (2004) UCSF Chimera--a visualization system for exploratory research and analysis. *Journal of computational chemistry* 25, 1605-1612
51. Signor, L., and Boeri Erba, E. (2013) Matrix-assisted laser desorption/ionization time of flight (MALDI-TOF) mass spectrometric analysis of intact proteins larger than 100 kDa. *J Vis Exp*
52. Kussmann, M., and Roepstorff, P. (2000) Sample preparation techniques for peptides and proteins analyzed by MALDI-MS. *Methods Mol Biol* 146, 405-424

Table 1. Crystallographic Parameters and Statistics for Chd^T (6UXU).

Data Processing	
Space group	P 2 ₁ 2 ₁ 2 ₁
Cell dimension	
α, β, γ (deg)	90, 90, 90
a, b, c (Å)	54.8, 105.2, 122.4
Processed Resolution (Å)	1.96
I/σ (I)	17.5 (1.1)
Resolution at I/σ (I) = 2 ^a	1.98
R _{merge} ^b (%)	8.7 (117.6) ^c
R _{pim} ^d (%)	2.7 (35.0)
CC ½ ^e (%)	(63.1)
Completeness (%)	98.0 (87.6)
Multiplicity	7.2
No. Reflections	362,906
No. Unique Reflections	50,386
Refinement	
R _{work} ^f /R _{free} ^g (%)	15.79/19.75
No. of Atoms	
protein	4,693
ligand	3
water	379
B factors (Å ²)	
protein	23.7
RMSD ^h	
bond lengths (Å)	0.010
bond angles (deg)	1.014
Ramachandran plot (%)	
most favored	96.14
allowed	3.19
outliers	0.67
^a Provided Resolution at I/σ = 2 for conventional assessment of data quality	
^b R _{merge} = Σ I _{obs} - I _{avg} /ΣI _{avg}	
^c The values for the highest-resolution bin are in parentheses	
^d Precision-indicating merging R	
^e Pearson correlation coefficient of two “half” data sets	
^f R _{work} = Σ F _{obs} - F _{calc} /ΣF _{obs}	
^g Five percent of the reflection data were selected at random as a test set, and only these data were used to calculate R _{free}	
^h Root-mean square deviation	

Table 2. Selected Bond lengths

Atom1	Atom2	Length (Å)
Active site Zn	Carboxylate oxygen atom of Asp116	2.1
Active site Zn	N ^ε nitrogen's of His117	2.0
Active site Zn	N ^ε nitrogen's of His257	2.0
Active site Zn	Carbonyl oxygen atom of Asn216	2.2
Active site Zn	Metal-bound water/hydroxide	2.6
N [⊥] nitrogen's of His114	Metal-bound water/hydroxide	2.9
N [⊥] nitrogen's of His114	Nitrogen atom of Asn216	2.7
N [⊥] nitrogen's of His114 (perpendicular)	Metal-bound water/hydroxide	5.4
N [⊥] nitrogen's of His114 (perpendicular)	Nitrogen atom of Asn216	3.1
Structural Zn	N ^ε nitrogen's of His143	2.0
Structural Zn	Carboxylate oxygen atom of Asp146	1.9

Figure Captions

Figure 1. Hydrolysis of TPN to 4-OH-TPN and chloride by Chd.

Figure 2. A) Homodimer of Chd^T. Three Zn(II) ions are shown as balls and the coordination residues are shown as sticks. B) A side view of the Chd^T homodimer, with defined “Top” and “Bottom” sides according to the relative positions to the structural Zn(II) ion.

Figure 3. A) Hydrophilicity surface map of the Chd^T dimer from the “bottom” side. The orange arrow indicates a single large opening. B) Surface view of the Chd^T dimer from the “top” side. The green arrows indicate two separate openings. C) Cross sectional view of the Chd^T dimer. The orange arrows indicate a “Y” shaped channel with access to the catalytic Zn(II) ions from the bottom side while the green arrows indicate one branch of the “Y” shaped channel that provides access to the catalytic Zn(II) from the “top”. The other “Y” shaped channel from the “top” side is on the backside of this view and was not visible.

Figure 4. A) The overall protein fold of a Chd^T monomer. The β -lactamase fold (residues 1-277) is in blue. A C-terminal motif (residues 278-327) is in red. B) Chd^T is superimposed with the β -lactamase CphA (PDB code: 3IOG), which is in magenta. C) Chd^T is superimposed with an SEC alkyl sulfatase (PDB code: 2YHE), which is in pink.

Figure 5. A) Chd^T active site. Zn(II)-ligand bonds are shown in gray sticks and hydrogen bonds are shown as black dashed lines. The key distances are shown in angstroms. The two alternate conformations of His114 are labeled as His114a and His114b. B) Simulated annealing composite omit maps ($2F_o - F_c$) are shown in grey mesh at the 1.0 sigma level for the coordinated residues, water, Zn(II), and His114. The residues are shown in the same orientations as that in A. C) The structural Zn(II) ion at the dimer interface. Zn(II)-ligand bonds are shown as gray sticks. One dimer is in tan, the other is in cyan. His143 and Asp146 from different subunits are indicated with “A” or “B”. D) The simulated annealing composite omit map ($2F_o - F_c$) is contoured at 1.0 sigma around the structural Zn(II) ion and its coordinated residues.

Figure 6. MALDI-TOF mass spectra of: A) truncated Chd^T (black) and the Chd^T double mutant (red).

Figure 7. Four TPN docking poses for the active site of Chd^T. The best pose (#1) indicates ligation of a CN group from TPN to the active site Zn(II) ion.

Figure 8. A revised catalytic mechanism for TPN hydrolysis by Chd.

Figure 1.

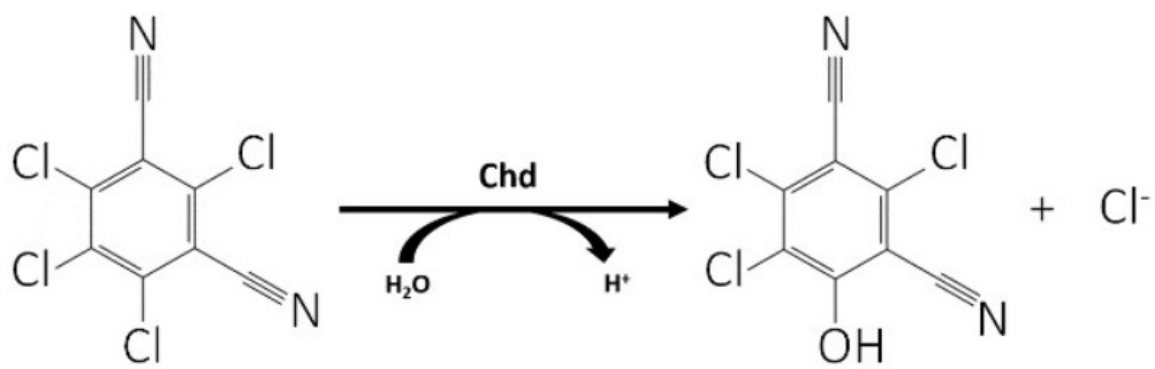


Figure 2.

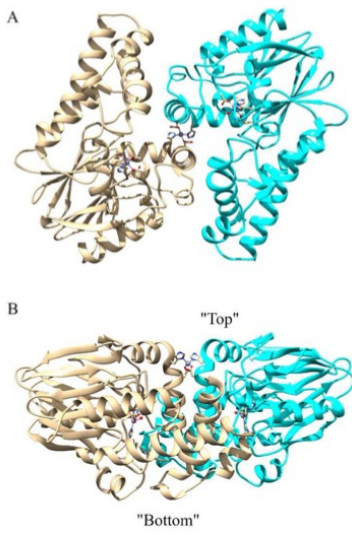


Figure 3.

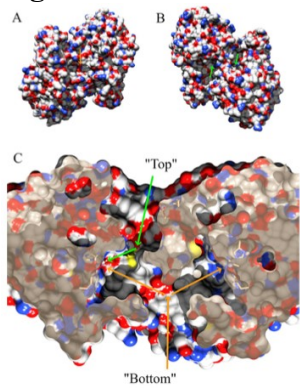


Figure 4.

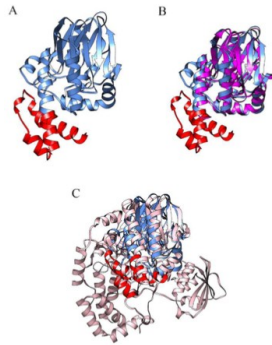


Figure 5.

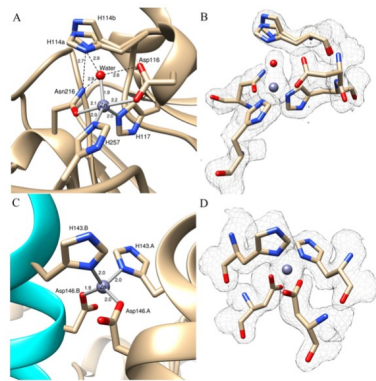


Figure 6.

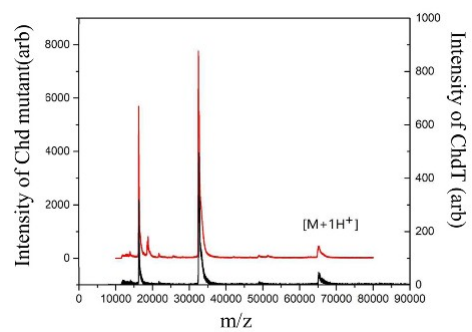


Figure 7.

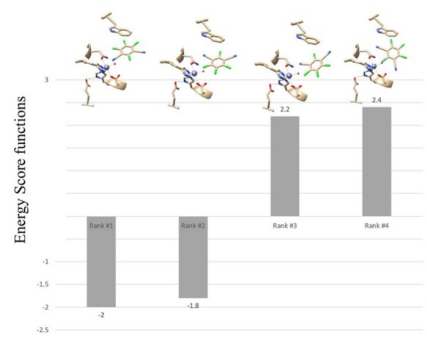
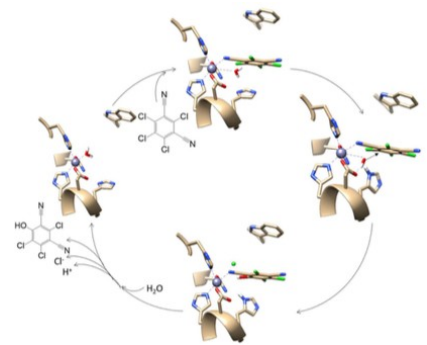


Figure 8.



Supplementary Information Figure S11. Size exclusion gel filtration chromatography curves of truncated Chd (solid line) and Chd mutant (dash line) by 50 mM HEPES buffer at pH 7 indicating both are homodimers in solution.

Figure S11. Size exclusion gel filtration chromatography curves of truncated Chd (solid line) and Chd mutant (dash line) by 50 mM HEPES buffer at pH 7 indicating both are homodimers in solution.

